Chapter 9

UPGRADE STUDIES

This chapter provides a summary of the preliminary upgrade studies I have performed on gFEX, an upgrade project introduced in ??.

The gFEX [1] subsystem of the ATLAS Level-1 (L1) calorimeter trigger (L1Calo) trigger is one of several modules designed as part of the Phase-I upgrade [2] to maintain trigger acceptance against increasing LHC luminosity in Run 3 (2021) and beyond. It is designed to enhance the selectivity of the L1 trigger and increase sensitivity to key physics channels, such as identifying boosted tops in the final state, a focus this thesis analysis. A key feature of gFEX is that the entire calorimeter is available in a single module, which enables the use of algorithms that can sscan the entire η range of the calorimeter, especially for calculating event-level observables. One of these full-scan algorithms can identify boosted hadronic topologies that are characteristic of new physics scenarios. For example, a gFEX trigger algorithm can capture the entire decay of a top quark which can, under a Lorentz-boosted topology, shower over a large area without any significant local energy deposits in a limited region of interest. Finally, the architecture of gFEX permits event-by-event local pile-up suppression, providing robust observables which reduced pile-up dependencies.

This chapter provides an overview of trigger analysis studies performed with the instrumentation upgrade that I have been involved with, gFEX. First, a strong physics motivation is described and how gFEX can potentially contribute to the trigger upgrades in section 9.1. The gFEX reconstruction algorithm used in the following studies is described in section 9.2. Next, section 9.3 discusses the necessary background to read and understand **turn-on curves**. A turn-on curve allows us to parameterize a given trigger in terms of the efficiency of selecting offline reconstructed objects. Once the necessary background is in place, a few preliminary studies (section 9.4) are shown, with lots of room for future improvement and continuation.

9.1 Motivating gFEX

Let's suppose, for example, we are performing a search for $Z'(\to t\bar{t})$ by identifying its decay products as shown in fig. 9.1. A jet is clustered from calorimeter clusters shown as black dots in the event display. Subjets are formed from topoclusters associated with the jet using the C/A algorithm with $R = 0.2$. The intial state radiation (blue) can contribute significantly to the amount of pile-up energy in this jet and reducing the resolution of measuring the jet. Finally, a black circle is drawn to help visualize the size of the $R = 1.0$ anti-k_t jet for the event while a purple rectangular box shows the size of the sliding window used in the Level-1 trigger algorithms online. As the Z' has a large amount of mass, the decay products ($t\bar{t}$) will have a significant Lorentz boost which makes it possible to observe the full top quark decay within a large-radius (large-R) jet.

As you've read about in **????**, high p_{T} Lorentz-boosted top quarks, W/Z/h bosons, and exotics are critical elements of the ATLAS physics program. As described in **??**, moving to an environment with more luminosity and more pile-up energy density will cause the trigger thresholds to go up to manage rates. gFEX is one of a series of instrumentation upgrades that will enable us to control the rates, while still being able to maintain an efficient trigger for such programs. As it's been made clear in fig. 9.1, the current Level-1 trigger uses a small sliding window which becomes inefficient for jets that decay over a larger area, exactly like the reconstructed objects I search for in this thesis analysis. Figure 9.2 shows the jet mass distribution for different physics processes: $t\bar{t}$, W/Z+jets and single top for Lorentz-boosted jets. A top quark, with $p_{\mathrm{T}} > 350\,\mathrm{GeV}$ will have approximately a size parameter $R \sim 2\frac{m}{p_{\mathrm{T}}} < 1.0$ and can be fully captured in a large-R jet. The white shows a fully-contained top inside an $R = 1.0$ anti-k_t jet that peaks around the mass of the top quark. A non-fully

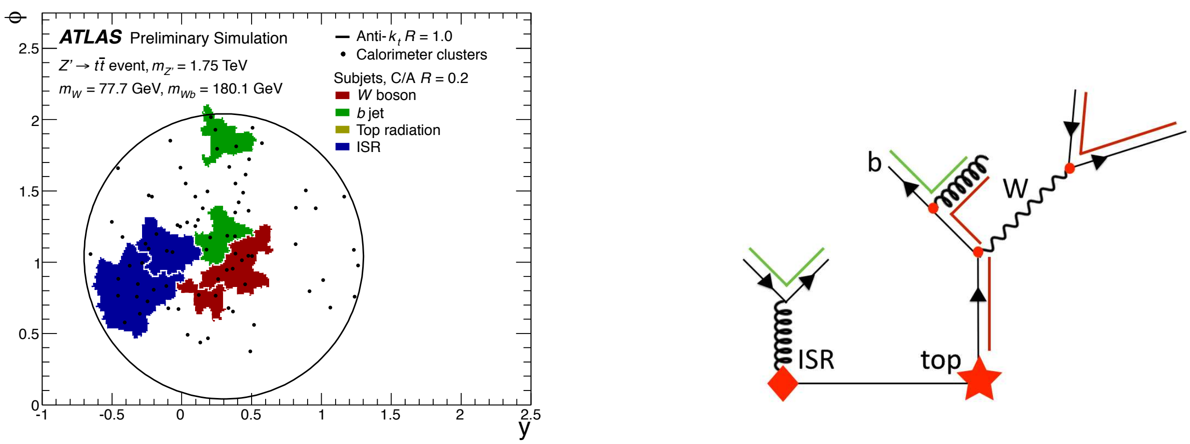

(a) Event Display (b) Shower History

Figure 9.1: [3] Illustration of a simulated large radius anti-k_t jet, with $R = 1.0$ from a top quark produced in a $Z' \rightarrow t\bar{t}$ decay with $m_{Z'} = 1.75\,\text{TeV}$. The (a) event display and (b) parton shower history for an example decay. Subjets are identified by a particular color in the event display: W boson (red), b-jet (green), top radiation (yellow), and initial state radiation (blue). Shown is a black circle representing the size of the $R = 1.0$ anti-k_t offline jet that is clustered and can capture the full information of the top decay and a dashed, purple rectangular window of size 0.8×0.8 representing the L1 trigger sliding window algorithm for identifying energy above a fixed threshold.

contained top has peaks around the invariant mass of the two quarks from the hadronic W-boson decay and the invariant mass of the b-jet and one of the quarks from the hadronic W-boson decay.

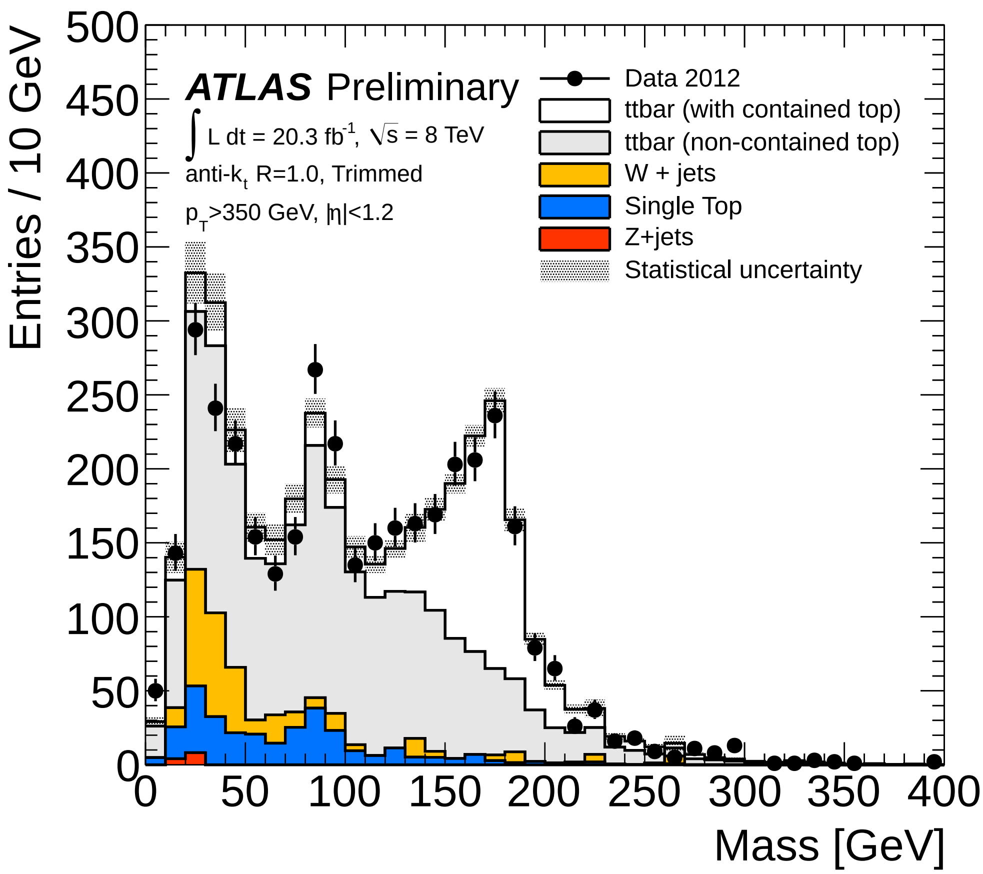

Figure 9.2: [4] Jet mass for leading p_{T} anti-k_t trimmed jets with $R = 1.0$, $|\eta| < 1.2$, and $p_{\mathrm{T}} > 350\,\mathrm{GeV}$. Here, "contained" refers to events having a hadronically-decaying top quark t with collimated daughter particles at the truth level (all three daughter quarks $q_i \equiv bq\bar{q}$ satisfy $\Delta R(q_i, t) < 1.0$). The shaded band represents the bin-by-bin statistical uncertainty in monte-carlo simulation.

This gives rise to the concept of substructure, which talks about a hadronic top quark being a three-pronged decay, while a hadronic W-boson is a two-pronged decay. As seen from the leading jet mass in fig. 9.2, the mass of a jet indiciates a measure of the amount of substructure inside. So if a jet with sufficient energy decays over too large of an area, the

Level-1 trigger will not fire, it cannot capture the full energy of the jet, and this sliding window algorithm is therefore **inefficient for jets with significant substructure**. In the next sections, we'll explore trigger studies and quantify the efficiency of the gFEX trigger compared to the Level-1 trigger for jets with substructure.

9.2 gFEX Algorithms

9.2.1 The reconstruction algorithm

The reconstruction algorithm is very primitive right now. Below, we provide a step-by-step process of how the jet is reconstructed. For each event

1. Filter the gTowers to only use those that pass a fixed E_{T} threshold. These are used to seed the algorithm.
2. For each seed, grab the gTowers around the seed satisfying

$$\Delta R \leq X \tag{9.1}$$

   or, in other words, a circle of radius ΔR centered around the seed.

3. We use ROOT's TLorentzVector class and add up the 4-vectors for all gTowers to the seed and use this to create our trigger object centered at the seed's geometric η, ϕ.

$$E_T^{\text{object}} = E_T^{\text{seed}} + \sum_{\text{towers around seed}} E_T^{\text{tower}} \tag{9.2}$$

Unless otherwise specified, large-R ($R = 1.0$) objects are the primary focus of this study, and the gFEX trigger. The area of a trigger jet is defined as the sum of the area of the gTowers included in the jet.

9.2.2 The Offline-Trigger Object Pairing Algorithm

In order to pair our objects, to help us understand how well our algorithm works with respect to a reference, such as offline reconstructed jets, we need to be able to match our reconstructed trigger objects with their corresponding offline reference object. For an event,

1. For each offline object - filter out the trigger objects so only trigger objects satisfying

$$\Delta R \leq X \tag{9.3}$$

2. From the "distance"-filtered trigger objects, identify the object with the highest E_{T} and use this as the offline event's paired object.

A typical cut is to apply $\Delta R < 1.0$ for reconstructed, isolated offline jets as gTowers are often colocated with the energetic jets as seen in fig. 9.3. A tighter ΔR cut can be applied if multiple energetic objects are within proximity of the leading offline jet, but these substructure-based studies will be discussed in section 9.4.3.

9.2.3 Event Displays

Figures 9.4 to 9.6 show example event displays for the (a) offline, reconstructed jets in the event, the (b) trigger jets formed from the reconstruction algorithm, and (c) the gTowers in the event for a $t\bar{t}$ monte-carlo simulated sample with center-of-mass energy $\sqrt{s} = 13\,\mathrm{TeV}$.

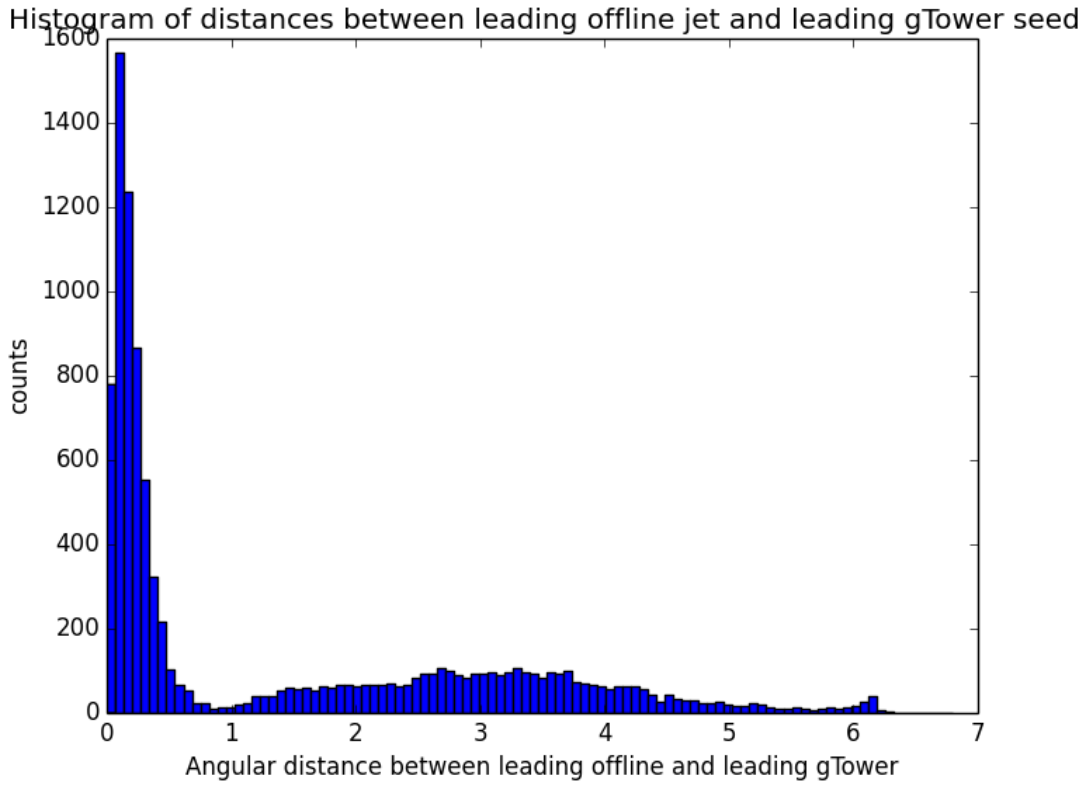

Figure 9.3: A distribution of the angular variable ΔR betwen the leading jet in the event and the leading gTower in the event for monte-carlo simulated $t\bar{t}$ samples with $\langle\mu\rangle = 80$ at a center-of-mass energy of $\sqrt{s} = 14\,\text{TeV}$. A majority of towers are found within $\Delta R < 1.0$ of the reconstructed, isolated offline jet in the event.

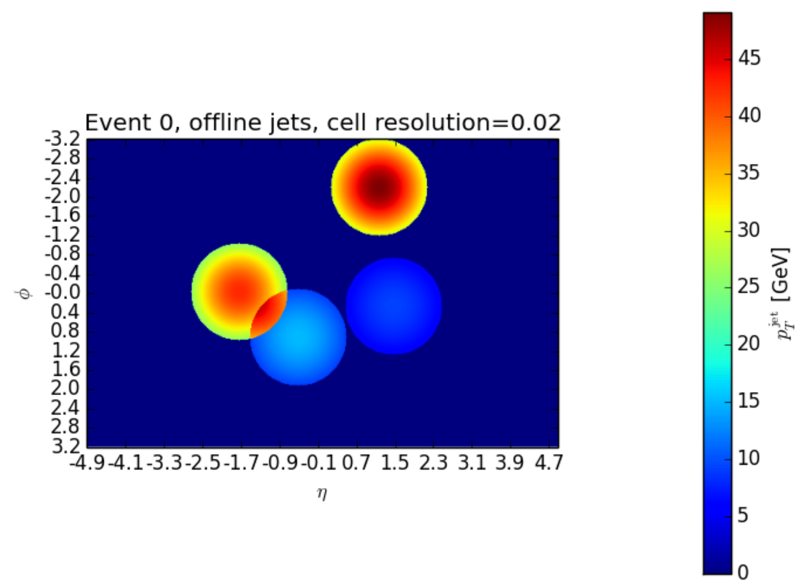

(a) offline jets

Figure 9.4: A canonical example that demonstrates the algorithms in the preceding subsections.

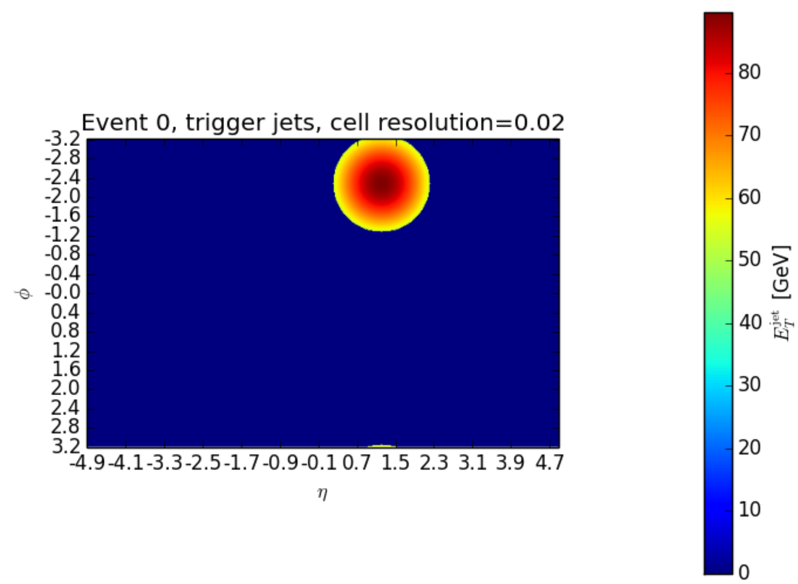

(b) trigger jets

Figure 9.4: A canonical example that demonstrates the algorithms in the preceding subsections.

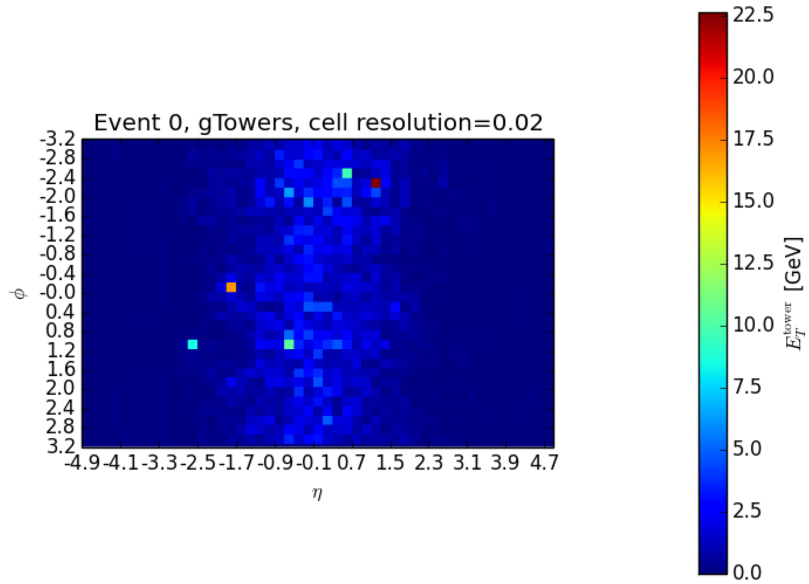

(c) gTowers

Figure 9.4: A canonical example that demonstrates the algorithms in the preceding subsections.

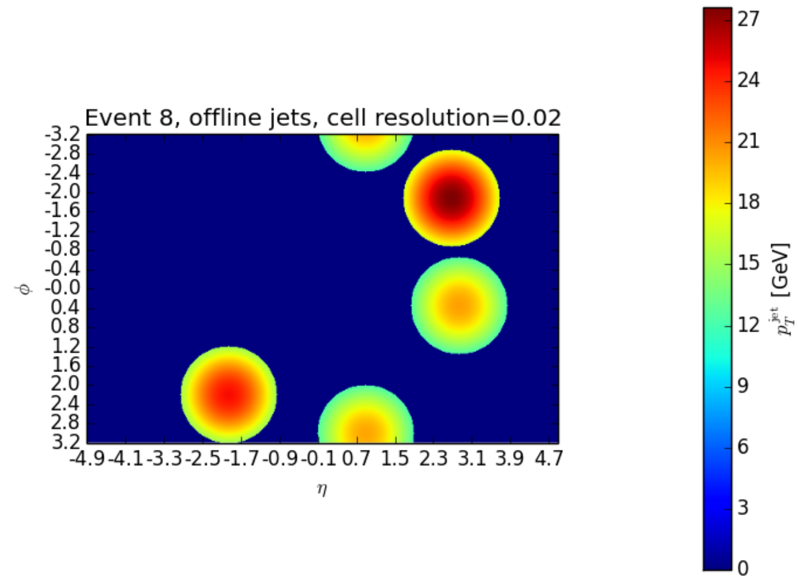

(a) offline jets

Figure 9.5: No gTowers were found for the given threshold of 20 GeV.

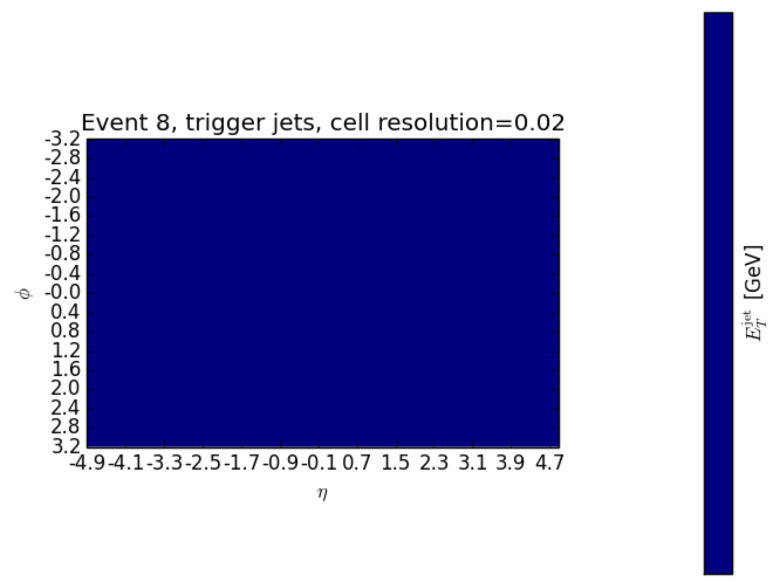

(b) trigger jets

Figure 9.5: No gTowers were found for the given threshold of 20 GeV.

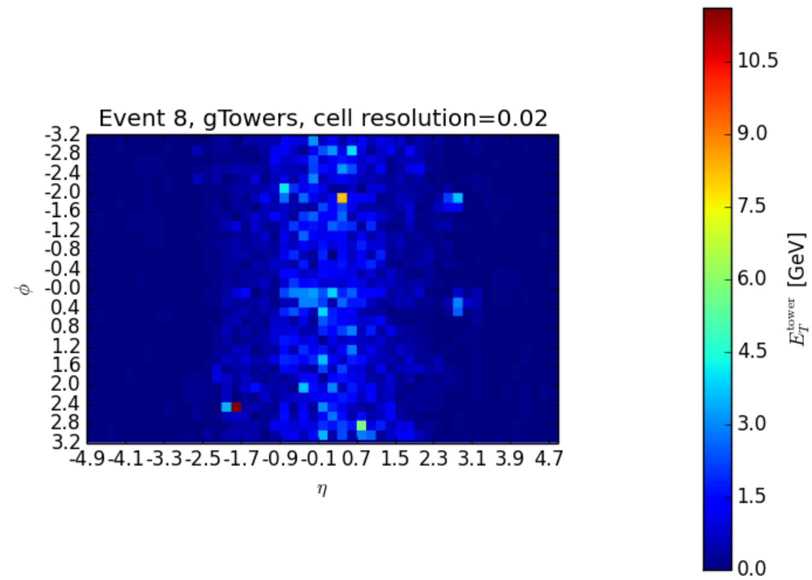

(c) gTowers

Figure 9.5: No gTowers were found for the given threshold of 20 GeV.

9.3 Efficiency of Triggers

Turn-on curves are one of the fundamental ways to quantify a trigger. One of the primary goals of the trigger is to maintain a high efficiency for offline reconstructed objects, based on how the trigger itself was designed. The calculation follows the formula eq. (9.4) where N^{offline} describes the distribution of offline objects before a trigger selection (subscript naught) and after a trigger selection (subscript $\mathcal{T}$).

$$\varepsilon_{\mathcal{T}} = \frac{N_{\mathcal{T}}^{\text{offline}}}{N_0^{\text{offline}}} \tag{9.4}$$

In terms of a technical implementation, you can generate a histogram of offline, reconstructed, leading jet p_{T} and then apply the trigger selection, and divide the two distributions bin-by-

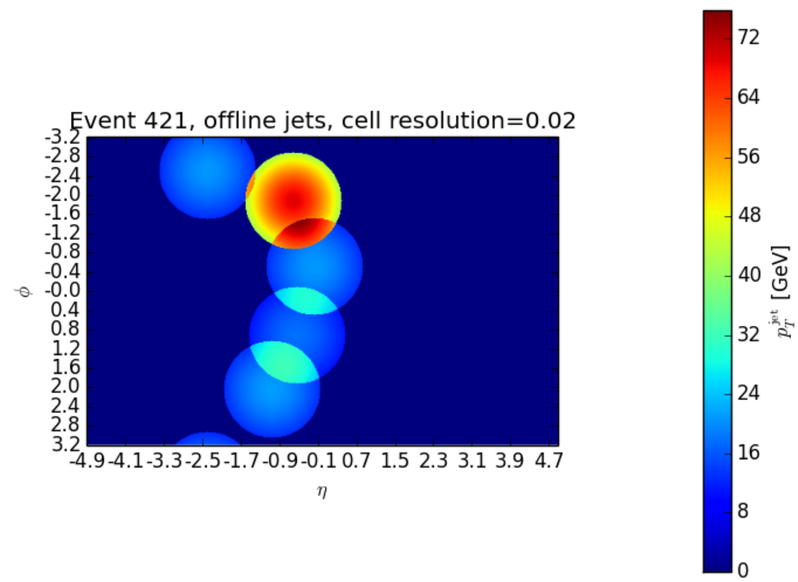

(a) offline jets

Figure 9.6: Overlapping gTowers with $E_{\mathrm{T}} > 20\,\mathrm{GeV}$ showing that even a crude version of a clustering algorithm is still able to identify at least two jets at almost identical locations.

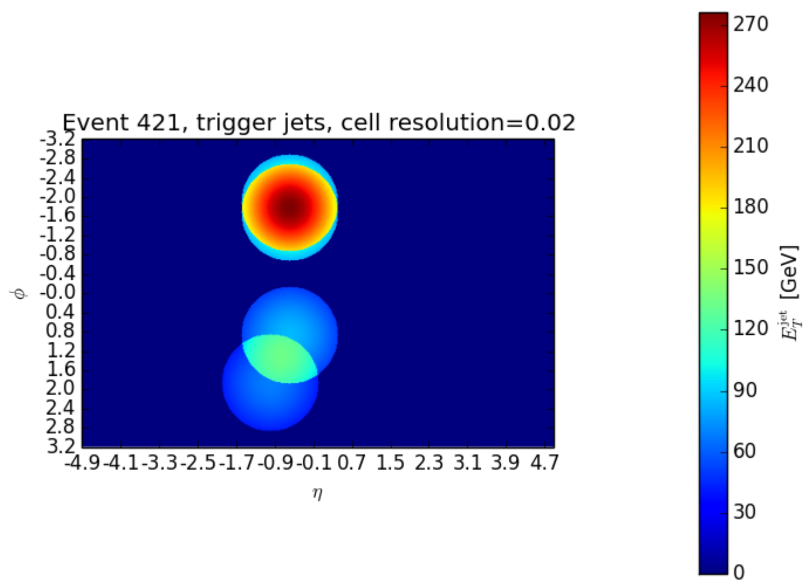

(b) trigger jets

Figure 9.6: Overlapping gTowers with $E_{\mathrm{T}} > 20\,\mathrm{GeV}$ showing that even a crude version of a clustering algorithm is still able to identify at least two jets at almost identical locations.

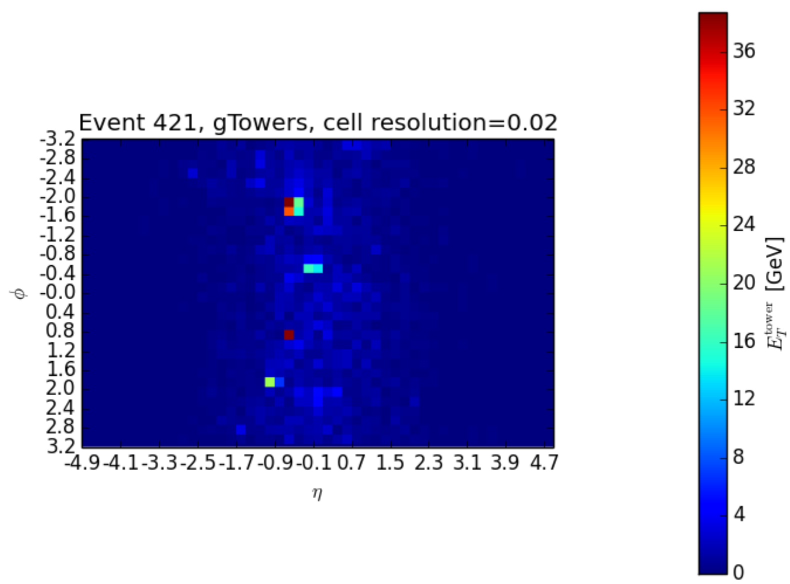

(c) gTowers

Figure 9.6: Overlapping gTowers with $E_{\mathrm{T}} > 20\,\mathrm{GeV}$ showing that even a crude version of a clustering algorithm is still able to identify at least two jets at almost identical locations.

bin. This approach is known as the differential approach as it divides in exclusive bins. An integral approach, as the name suggests, divides the cumulative versions of the histograms, bin-by-bin. In gFEX, a typical turn-on curve compares a selection using trigger objects such as gTowers, gBlocks against the offline, reconstructed, jets. Let's take an illustrative example with distributions shown in fig. 9.7, where dividing each trigger-selected distribution (b-d) by the one with no trigger selection (a) produces familiar turn-on curves fig. 9.8.

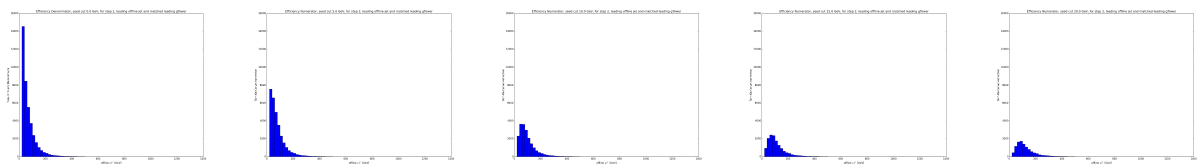

(a) no selection (b) 5 GeV (c) 10 GeV (d) 15 GeV (e) 20 GeV

Figure 9.7: Example distributions of reconstructed, uncalbrated, leading, anti-k_t $R = 1.0$ offline jet p_{T} (a) without a trigger selection applied and (b-d) a requirement on the leading gTower E_{T}. Offline jets are matched to the leading gTower in an event, so this amounts to an event-level trigger selection. The y-axis is the number of events. Turn-on curves from dividing each trigger-selected distribution by the denominator (no selection) is shown in fig. 9.8.

Each turn-on curve can be parameterized, or quantified, by two numbers: the resolution and the plateau location. The resolution of a turn-on curve is a measure of how sharply it "turns on". A trigger with better resolution turns on more sharply, therefore, the width of the turn-on region is smaller, and this is a good proxy for the resolution. The plateau location is the position along the x-axis where the turn-on reaches large efficiency, typically 95% efficiency. The quantification of turn-on curves allows one to be able to quickly visualize the performance of different trigger selections with two numbers that fully describe the turn-on. Figure 9.9 shows an example of three different turn-on curves, part of a study described more later in section 9.4, to demonstrate how the quantification of the resolution and the plateau can help compare trigger efficiencies. This quantification is useful as one is not easily able to see which of the three curves (red, blue, green) have the best resolution.

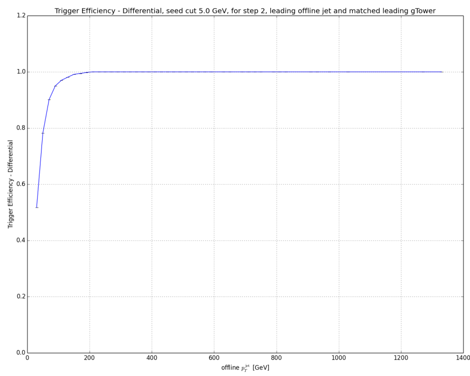

(a) 5 GeV

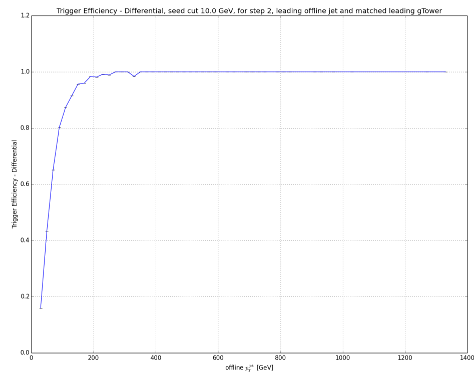

(b) 10 GeV

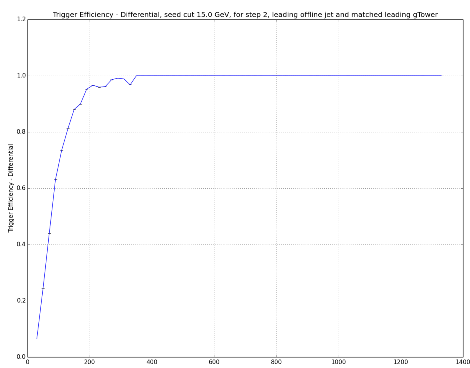

(c) 15 GeV

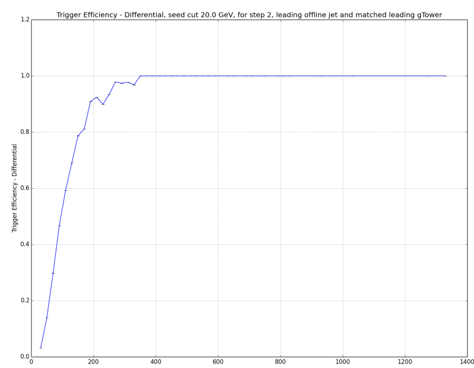

(d) 20 GeV

Figure 9.8: Example turn-on curves of reconstructed, uncalbrated, leading, anti-k_t $R = 1.0$ offline jet p_{T} with a requirement on the leading gTower E_{T}. Offline jets are matched to the leading gTower in an event, so this amounts to an event-level trigger selection. The y-axis is the efficiency of the trigger. These curves were calculated from distributions in fig. 9.7.

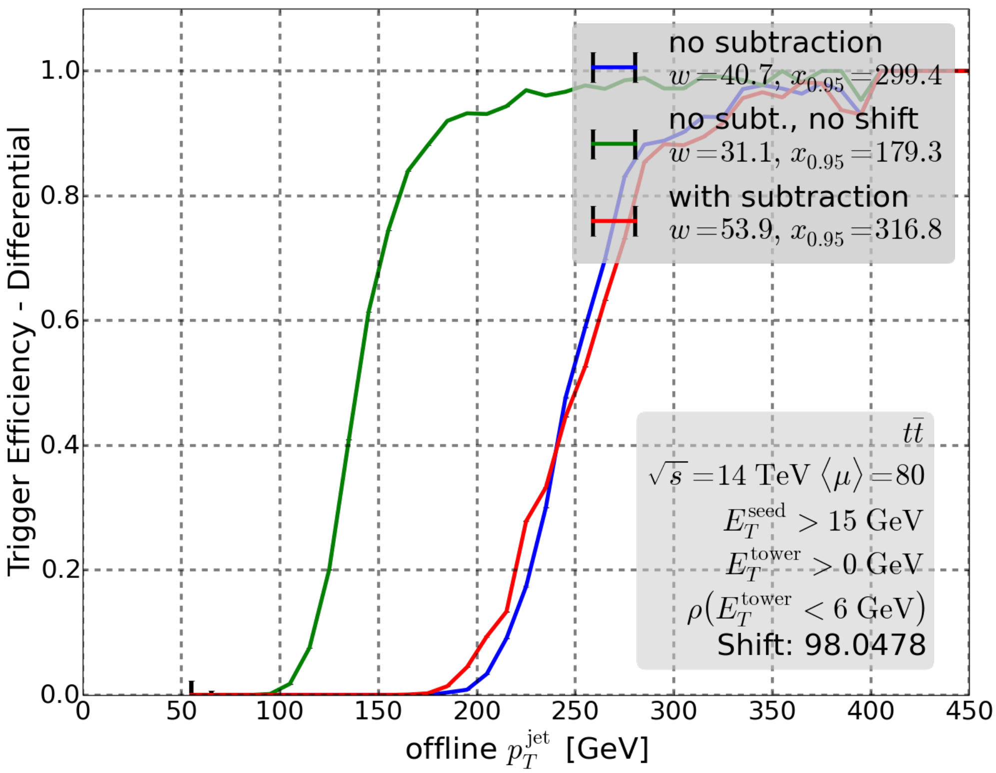

Figure 9.9: Example turn-on curves of different triggers to understand the impact of changes in the gFEX jet reconstruction algorithms for monte-carlo simulated $t\bar{t}$ events with center-of-mass energy $\sqrt{s} = 14\,\text{TeV}$, requiring the leading trigger jet to have $p_{\text{T}} > 140\,\text{GeV}$. The gFEX jet reconstruction algorithm is seeded by a 15 GeV gTower to form gFEX trigger jets. The green curve represents the efficiency of this standard reconstruction. The red curve represents the efficiency of the trigger jets, after they have been corrected for estimated pile-up energy density in the event, described more in section 9.4.1. Because there was an observed shift in the location of the trigger curve, the blue curve represents the efficiency using uncorrected trigger jets, but tightens the trigger selection from 140 GeV to 240 GeV (a shift of 98 GeV), to closely match the location of the red curve and understand the impact on the resolution of the trigger. Each turn-on curve is parameterized by the resolution w and the plateau $x_{0.95}$: green is $(w, x_{0.95}) = (31.1, 179.3)$, blue is $(w, x_{0.95}) = (40.7, 299.4)$, and red is $(w, x_{0.95}) = (53.9, 316.8)$.

So now that the foundation is laid out, fig. 9.10 shows the gFEX trigger using a $t\bar{t}$ monte-carlo simulated sample in a center-of-mass energy $\sqrt{s} = 14\,\text{TeV}$ which is expected for Run 3. There are two colors representing the two different triggers, red for the inclusive gFEX jet trigger and blue for the L1 inclusive jet trigger. For each color, there are three curves with different marker shapes representing the number of reconstructed subjets on the isolated, offline reconstructed jet matched to the corresponding trigger jet. Circles are offline jets with a single subjet, squares are offline jets with two subjets, and triangles are offline jets with three or more subjeets. As also shown in fig. 9.2, the number of subjets in the offline reconstructed jet corresponds very well with the particular physics process, such as a top quark hadronic decay or a hadronic W-boson decay. Therefore, one can think of circle markers representing dijet events, square markers representing hadronic W-bosons, and triangles representing top quarks. For an offline jet with a single subjet, both the L1 trigger and gFEX triggers have similar resolution[1] with a similar 99% plateau point[2] around 200 GeV. So the gFEX matches the behavior of the L1 trigger. When requiring that the offline jet has two or more subjets, the gFEX trigger is able to maintain the same resolution with the same plateau location, while the L1 trigger sees degraded performance. To put this in context for a physics analysis that depends on an inclusive jet triger, using the L1 trigger `L1_J100` would require the offline, $R = 1.0$ anti-k_t jets to have $p_{\mathrm{T}} > 200\,\text{GeV}$ to stay in the region of a fully-efficient trigger, provided that the jet has one subjet. If the jet has more substructure, a significantly tighter cut of $p_{\mathrm{T}} > 500\,\text{GeV}$ needs to be applied just to stay in the region of a fully-efficient trigger. Jets in a moderately boosted regime, from $p_{\mathrm{T}} > 200$–$500\,\text{GeV}$ would not be efficiently selected by the current L1 trigger, but would be covered by the proposed gFEX trigger. These jets are crucial to physics programs, such as the analysis

[1]The resolution is determined by the width of the slope of the turn-on curve. A sharper turn-on curve indicates better offline resolution.

[2]On a turn-on curve, one identifies the plateau by the x-value such that the efficiency is approximately 99%. A trigger with a lower plateau is more preferred as it reduces the selections needed to be applied on the offline object.

search presented in this thesis.

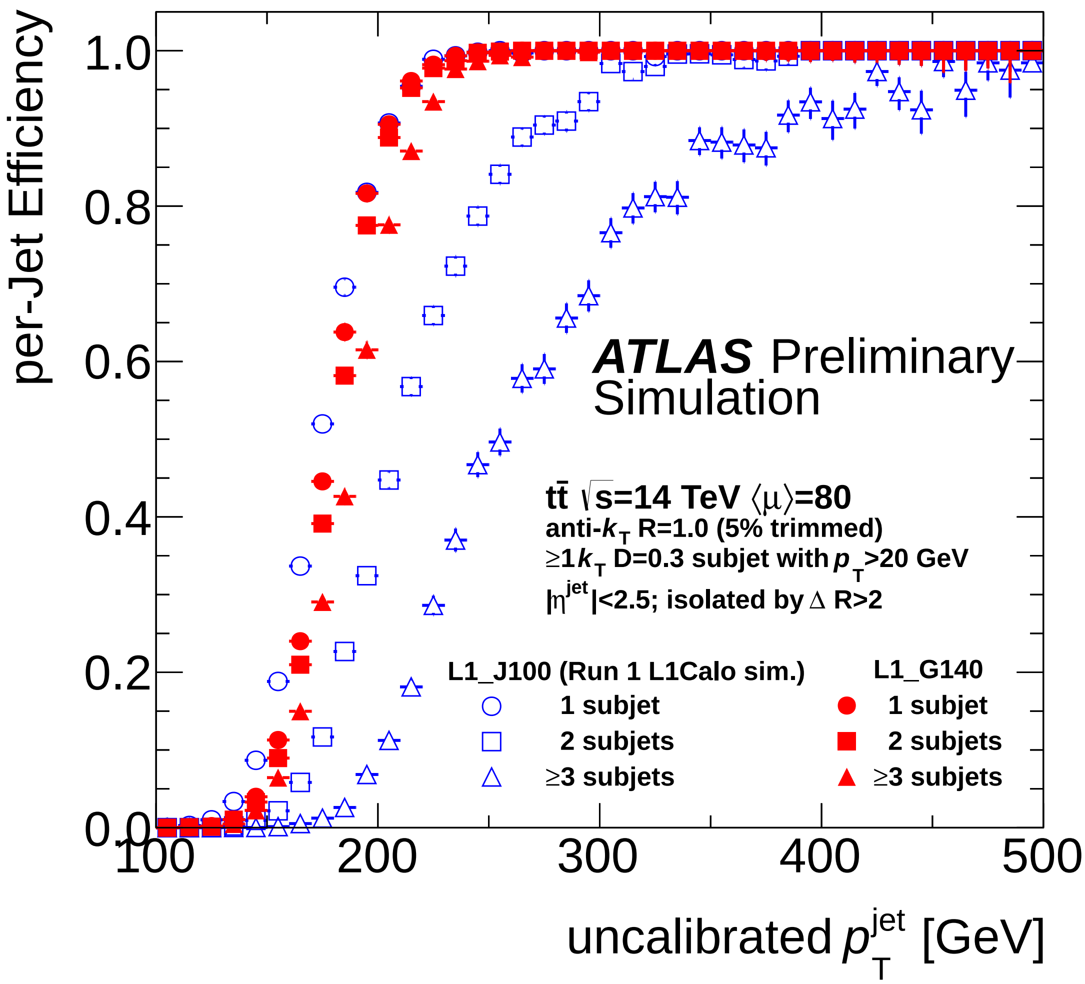

Figure 9.10: [5] Per-jet efficiency turn-on curves in Monte Carlo (MC) simulation for multiple Phase I upgrade Level-1 jet trigger options. A global feature extraction (gFEX) reconstruction algorithm (closed red markers, left) from the TDAQ Phase I Upgrade Technical Design Report (TDR) [6] with a 140 GeV threshold is compared to full simulation of the Run I Level-1 calorimeter jet trigger (open blue markers, left and right) with a 100 GeV threshold. The gFEX reconstruction implements a simple seeded cone algorithm with a nominal radius of $R = 1.0$ and with a seed selection of 15 GeV applied to calorimeter towers with area 0.2×0.2 in $\eta \times \phi$. The 140 GeV gFEX trigger threshold is chosen to match the `L1_J100` single subjet turn-on curve. Pair-produced top quark monte-carlo simulation samples are simulated with a pile-up level equivalent to an average number of interactions per bunch-crossing $\langle\mu\rangle = 80$. For each algorithm, the efficiency curves are shown as a function of the offline trimmed anti-k_t $R = 1.0$ jet p_{T} with different offline subjet multiplicities. The trimming parameters specify that any subjets with a p_{T} fraction of the original jet less than 5% are to be discarded. The subjets are defined using the k_t-clustering algorithm with a nominal radius parameter of $D = 0.3$. For subjet counting, the subjets are required to have a subjet $p_{\mathrm{T}} > 20$ GeV. The offline trimmed jets are required to be isolated from any other offline jet by at least a radial distance of $\Delta R > 2.0$ rad and to be within the pseudorapidity range $|\eta| < 2.5$. The turn-on curves measure per-jet efficiencies after requiring a that the the Level-1 gFEX jet be within $\Delta R < 1.0$ of the offline trimmed jet.

9.4 gFEX Studies

9.4.1 Pile-up Energy Density Calculations

As described in **????**, pile-up energy density is an important quantity to estimate for events at the Large Hadron Collider (LHC) where one can expect to see many interactions per bunch crossing as well as in the future of the LHC program, the HL-LHC, which could see up to 200 interactions! Being able to estimate pile-up at the trigger level is crucial for gFEX jet reconstruction and having this quantity calculated as early as possible in the collision helps downstream algorithms, such as those in the High-Level Trigger (HLT) perform more efficiently. This section describes a series of studies performed in order to estimate the offline pile-up in gFEX, which I will call **online pile-up**.

A hardware consideration is the latency constraints described in **??** which only allow up to five bunch crossings to run algorithms on gFEX. While the pileup calculation done offline uses a median-based approach, gFEX does not have enough time to sort 1284 gTowers in order to compute the pile-up. It also does not have enough time to form trigger jets and calculate pile-up using those jets. However, all is not lost, as a truncated-mean-based approach can work. This is described in eq. (9.5) which only considers pileup by summing gTowers below a particular energy threshold.

$$\rho_{\text{online}} = \text{mean}\left\{\frac{E_{\text{T}}^{i}}{\text{area}_i}\right\}, \forall i \in \text{gTowers with } E_{\text{T}} < X\,\text{GeV} \tag{9.5}$$

Figure 9.11 shows some distributions made for a study to explore the truncated-mean-based approach described in eq. (9.5) with two upper thresholds at 3 GeV and 6 GeV. Various upper thresholds were studied in steps of 1 GeV from 1 GeV to 15 GeV and two are chosen to be shown. The red curve corresponds to using all gTowers, the teal and magenta curves are for the negative and positive central region respectively, and the gold and black are for the negative and positive forward region respectively.

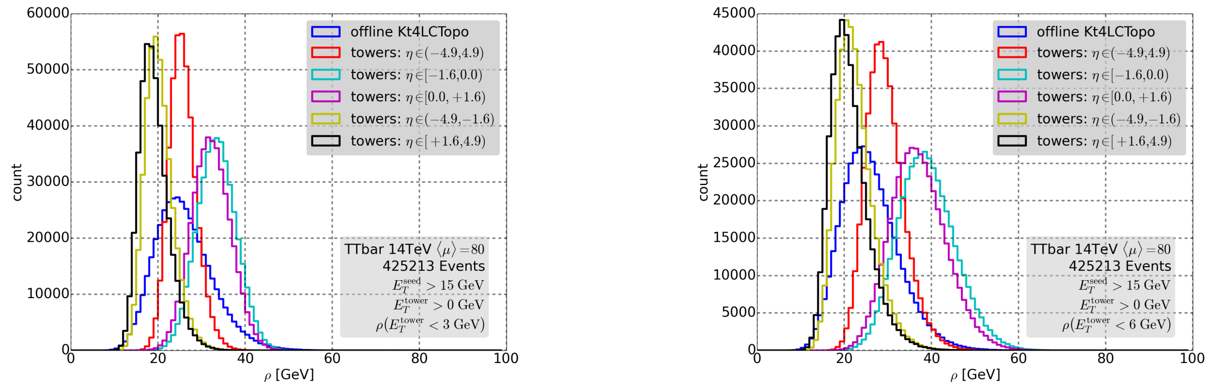

(a) $X < 3\,\mathrm{GeV}$

(b) $X < 6\,\mathrm{GeV}$

Figure 9.11: Distributions of truncated-mean-based online pile-up calculation using gTowers across different η ranges compared to offline pile-up (blue) for monte-carlo simulated $t\bar{t}$ events with $\langle\mu\rangle = 80$ at center-of-mass energy $\sqrt{s} = 14\,\mathrm{TeV}$. While the scale is not important as this can be calibrated later, the width of each distribution is and how well it corresponds to offline. The upper threshold, X, also labeled on the plot as $\rho(E_T^{\mathrm{tower}} < X\,\mathrm{GeV}$, is also specified as (a) $3\,\mathrm{GeV}$ and (b) $6\,\mathrm{GeV}$.

Figure 9.12 shows the first of these successful studies demonstrating the efficacy of the truncated-mean-based calculation of online ρ using central[3] gTowers for two different monte-carlo simulated samples. Both samples have an average interaction per crossing $\langle\mu\rangle = 80$ at center-of-mass energy $\sqrt{s} = 14\,\mathrm{TeV}$. The online pile-up is shown to be strongly correlated to the offline pile-up, ignoring a difference in the scales which is expected as the gTowers have not been calibrated. The very nice conclusion is that the online calculation of ρ is independent of the physics processes we're studying. By definition, ρ should not depend on the hard scatter and it does not! Upper thresholds were explored in steps of $1\,\mathrm{GeV}$ from $1\,\mathrm{GeV}$ to $15\,\mathrm{GeV}$, $X = 6\,\mathrm{GeV}$ was found to have the strongest correlation.

[3]The gTowers selected correspond to an η range of the original proposal of gFEX. These studies will need to be updated again using current monte-carlo simulation upgrade samples and an updated η range.

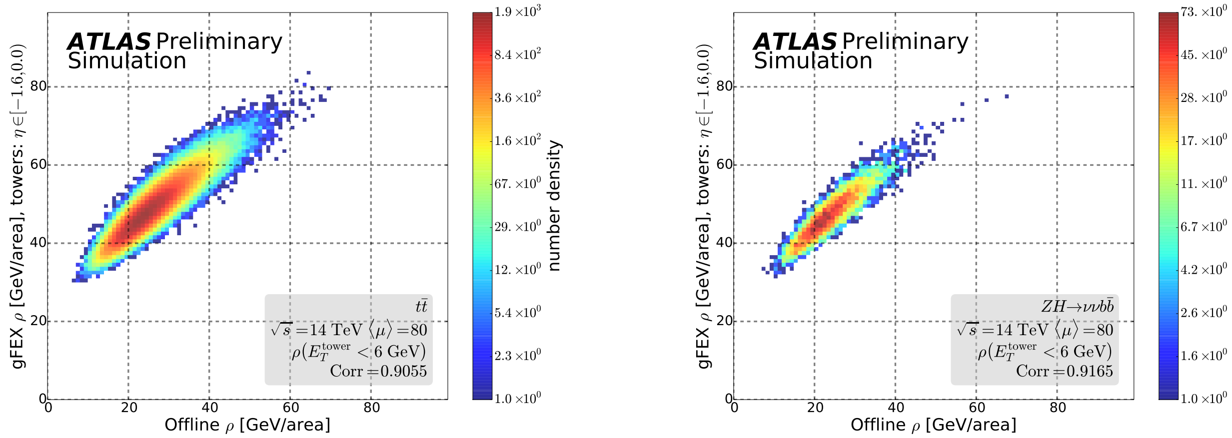

(a) $t\bar{t}$ (b) $ZH \to \nu\nu b\bar{b}$

Figure 9.12: [5] Correlation between the offline event energy density ρ [7] on the horizontal axis and a simplified calculation of the event energy density in the L1Calo trigger using gFEX with a truncated-mean-based approach using gTowers with $E_T^{\text{tower}} < 6\,\text{GeV}$ and $-1.6 < \eta < 0.0$. The correlation for (a) $t\bar{t}$ and (b) $ZH \to \nu\nu b\bar{b}$ events is greater than 90%. Both monte-carlo simulation samples are simulated with average number of interactions $\langle\mu\rangle = 80$ at a center-of-mass energy $\sqrt{s} = 14\,\text{TeV}$. In each case, the strong correlation means that the average value of ρ measured by the gFEX trigger for a given offline ρ is similar.

9.4.2 Pile-up Mitigation Studies

The next set of studies is a natural continuation from the pile-up calculation studies in section 9.4.1 by focusing on the effects of incorporating pile-up calculations in the gFEX trigger efficiency. Do we lose resolution? Do we see performance gains? Using the trigger jet reconstruction algorithm described in section 9.2 to build gFEX trigger jets with $R = 1.0$, an area-based mitigation approach is taken to subtract pile-up from the jet. This is described in eq. (9.6) which corrects the energy of a jet based on the area of the jet.

$$E_T^{\text{jet, corr.}} = E_T^{\text{jet}} - \rho_{\text{online}} \times \text{area}^{\text{jet}} \tag{9.6}$$

Using this area-based pile-up mitigation, fig. 9.13 shows the correlation betwen the offline jet and online jet energies before and after the correction. What is interesting to note is that while the scale of the trigger jets has expectedly and notably shifted downwards, the correlation between the offline jet energy and trigger jet energy remains just as strong. At low energies, there was a slight non-linearity observed before the correction that seems to be partially linearized after the pile-up correction is applied. Further study is needed here.

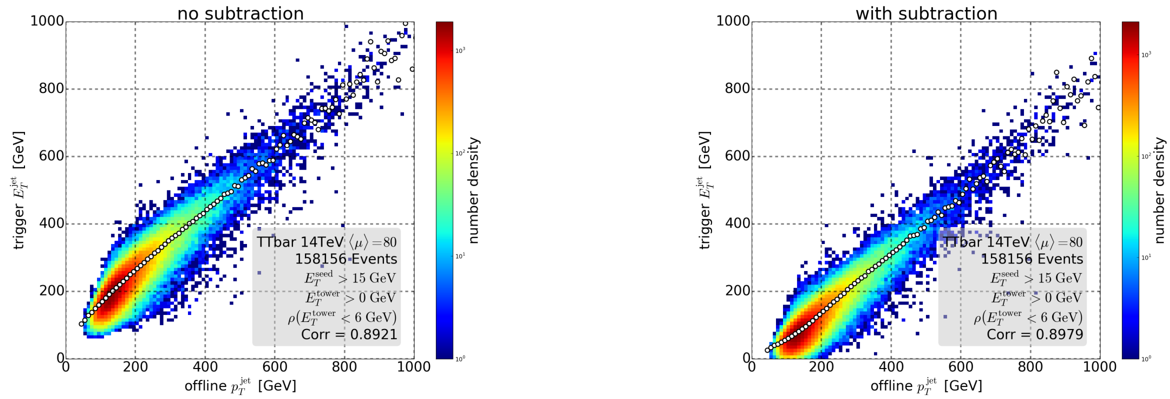

(a) no mitigation

(b) with mitigation

Figure 9.13: Correlation between isolated offline jet and matched gFEX trigger jet energies for $-1.6 < \eta < 0.0$ in a monte-carlo simulated $t\bar{t}$ sample with $\langle\mu\rangle = 80$ at a center-of-mass energy $\sqrt{s} = 14\,\mathrm{TeV}$. The correlations are shown (a) before and (b) after pile-up mitigation is applied. The trigger jets were seeded using towers with $E_\mathrm{T} > 15\,\mathrm{GeV}$ and the truncated-mean-based pile-up ρ_online was calculated using towers with $E_\mathrm{T} < 6\,\mathrm{GeV}$ which was optimized. The white circles represent the average trigger jet energy in each offline jet bin.

The next study was to determine how the pile-up correction improved the resolution of the trigger jets with respect to the matched, isolated offline jet as shown in fig. 9.14. The resolution calculation (eq. (9.7)) describes how well the online trigger jet measures the matched, isolated, offline reconstructed jet. Figure 9.14 shows correlation plots of the resolution of trigger jets as a function of the matched, isolated offline jet p_T before and after pile-up mitigation. While there is still significant non-linearity after pile-up mitigation, pile-up mitigation significantly improves the resolution of the trigger jets for offline jets with $p_\mathrm{T} > 250\,\mathrm{GeV}$ which is right in the region that gFEX is designed to specialize in. Moreover, there is no non-linearity before any pile-up mitigation which makes it very difficult to calibrate the energy of the trigger jets. Figure 9.15 shows y-projections of the trigger jet resolution in a few selected offline jet p_{T} ranges before and after the pile-up mitigation. The pile-up mitigation does not negatively affect the width of the distribution of trigger jets for lower energy offline jets with $p_{\mathrm{T}} < 250\,\mathrm{GeV}$ but does measurably narrow the distribution of trigger jets for offline jets with $p_{\mathrm{T}} > 300\,\mathrm{GeV}$.

$$\mathcal{R} = \frac{E_T^{\text{gFEX jet}} - p_{\mathrm{T}}^{\text{offline jet}}}{p_{\mathrm{T}}^{\text{offline jet}}} \tag{9.7}$$

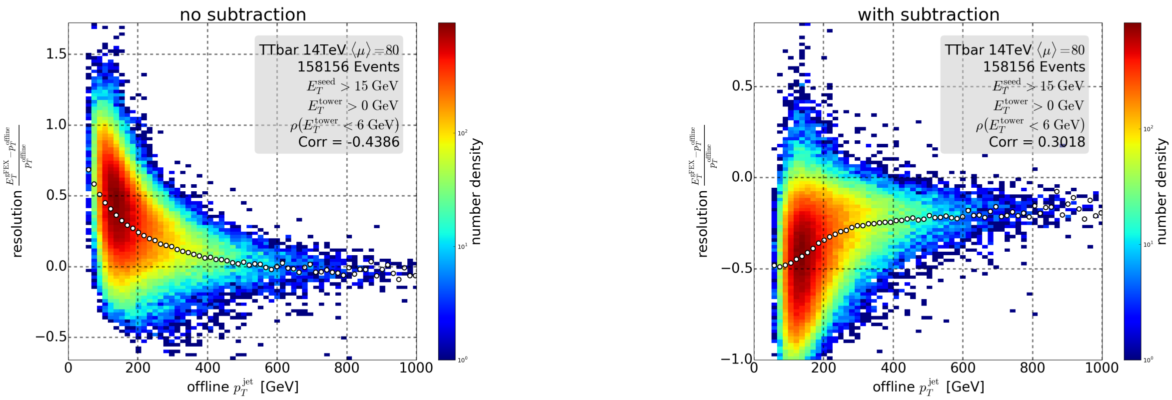

(a) no mitigation (b) with mitigation

Figure 9.14: Correlation between isolated offline jet and the energy resolution of the matched gFEX trigger jet is shown for $-1.6 < \eta < 0.0$ in a monte-carlo simulated $t\bar{t}$ sample with $\langle\mu\rangle = 80$ at a center-of-mass energy $\sqrt{s} = 14\,\mathrm{TeV}$. The resolutions are shown (a) before and (b) after pile-up mitigation is applied. The trigger jets were seeded using towers with $E_{\mathrm{T}} > 15\,\mathrm{GeV}$ and the truncated-mean-based pile-up ρ_{online} was calculated using towers with $E_{\mathrm{T}} < 6\,\mathrm{GeV}$ which was optimized. The white circles represent the average resolution in each offline jet bin. The resolution of the trigger jet energy is defined as a measure of the difference with respect to the matched offline jet compared to the energy of the offline jet.

Finally, the last study for pile-up mitigation is a question of how much energy is being subtracted from each trigger jet shown in fig. 9.16.

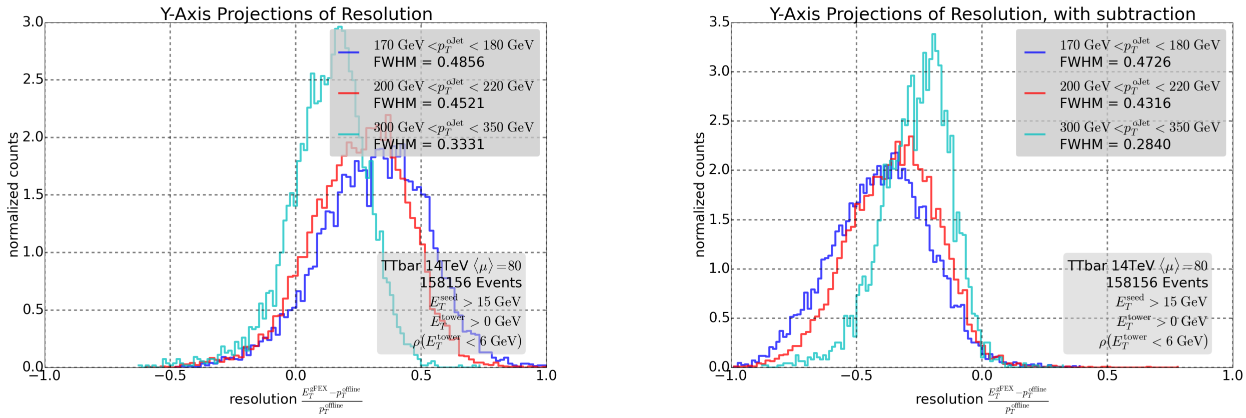

(a) no mitigation

(b) with mitigation

Figure 9.15: Y-axis Projections of the resolution plots in fig. 9.14 for selected offline jet p_T ranges: 170–180 GeV, 200–220 GeV, and 300–350 GeV. This was done on monte-carlo simulated $t\bar{t}$ events with $\langle\mu\rangle = 80$ at a center-of-mass energy $\sqrt{s} = 14$ TeV. The projections are shown (a) before and (b) after pile-up mitigation is applied. Each legend also reports the full-width half-max (FWHM) of a Gaussian fit to each of the projections, a smaller value being a stronger resolution.

Efficiency of Pile-up Mitigation Techniques

Thus far, there has been demonstrated, significant studies into the area-based pile-up mitigation techniques. However, up until now, no turn-on curves have been shown to demonstrate these. An area-based subtraction is indeed possible. Other choices for reducing pile-up are

- **noise cut**: a simple selection removing towers below a certain threshold
- **hybrid cut**: a combination of a noise cut at 3 GeV and applying 25% of the area-based pile-up subtraction ($0.25\rho_\text{online}$)

A study was proposed and done to study the impact of all of these different pile-up mitigation techniques on the trigger efficiency for a fixed trigger selection shown in fig. 9.17[4]. For each curve, the resolution (width of turn-on w) and the plateau location $x_{0.95}$ is reported. It is

[4]These studies need to be redone with equal rate settings.

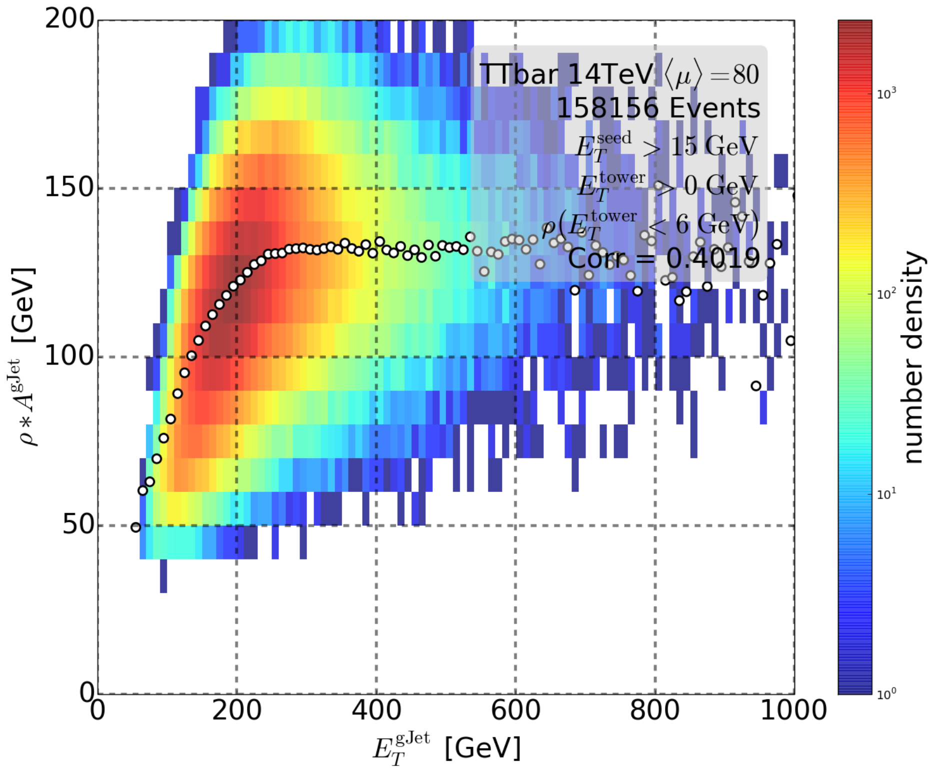

Figure 9.16: Correlation showing the amount of pile-up energy density subtracted from a given trigger jet as a function of the matching, isolated offline reconstructed jet for $-1.6 < \eta < 0.0$. This was done on monte-carlo simulated $t\bar{t}$ events with $\langle\mu\rangle = 80$ at a center-of-mass energy $\sqrt{s} = 14\,\text{TeV}$. For offline jets below 200 GeV, there are usually not enough energetic gTowers around the seeded tower with $E_{\text{T}} > 15\,\text{GeV}$ to be included in the reconstruction and so those associated, lower energy trigger jets tend to be smaller in area as they have less towers and so the correction falls off with energy. At a certain point, the correction is approximately the same which is the "full-occupancy" trigger jet with all gTowers within $\Delta R < 1.0$ of the seed participating in the reconstruction. For enough energy,

seen that a hybrid cut tends to have measurably better resolution than just an area-based subtraction alone, but the noise cut appears to have the largest impact on the resolution of a trigger jet. This is expected as the noisy towers can smear the resolution of a jet energy. Further selections applied on the offline jet mass to enhance the hadronic W-bosons (fig. 9.18) and hadronic tops (fig. 9.19) are also shown with very similar conclusions.

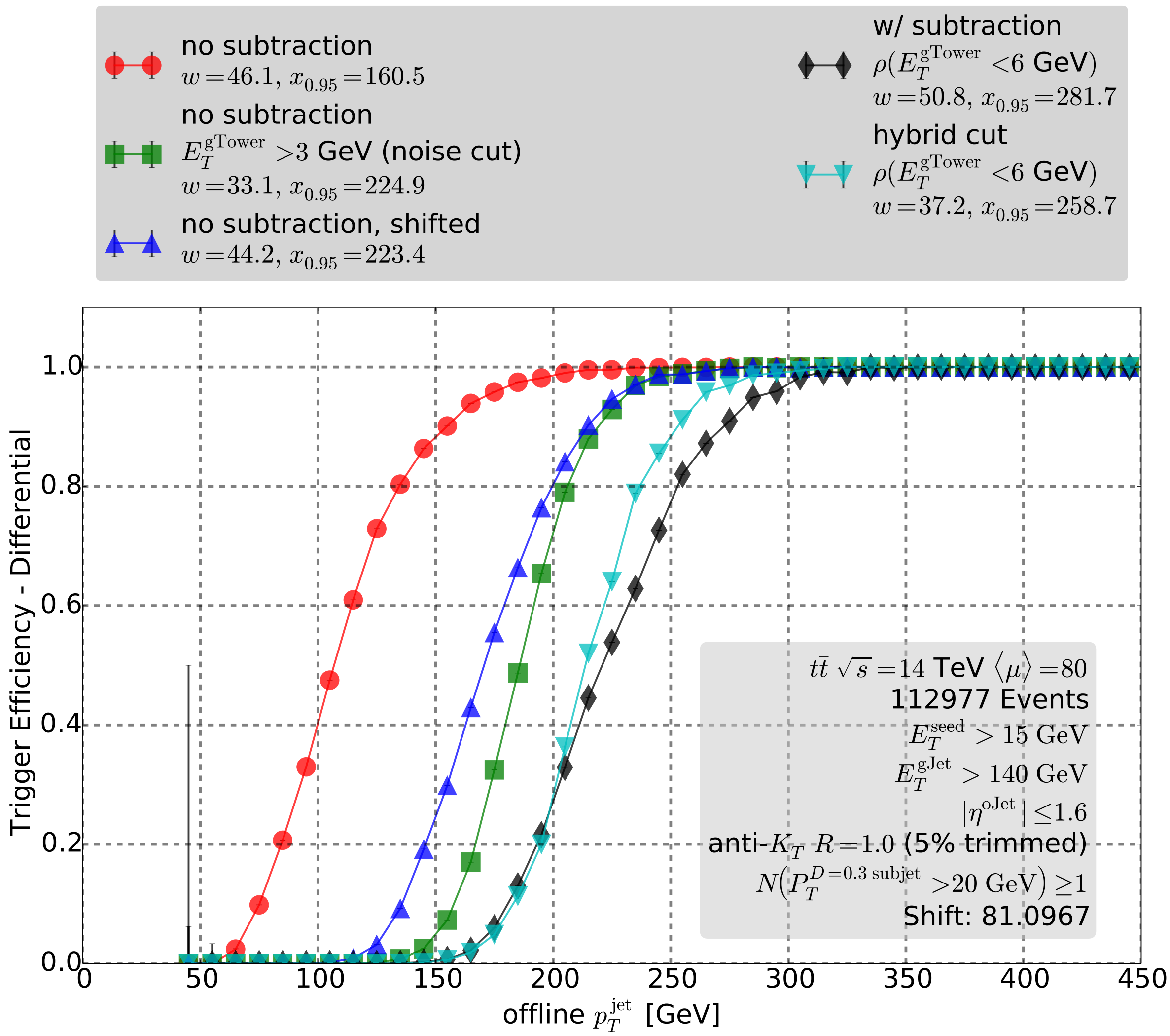

Figure 9.17: Trigger efficiency curves for the five different pile-up mitigation techniques. These are: no subtraction, no subtraction but a noise cut applied, no subtraction and simply shifted, with pile-up subtraction, and a hybrid cut. The legend reports the width of the turn-on w and the location of the plateau at 95% $x_{0.95}$. The efficiency is reported as a function of the large-R $R = 1.0$ anti-k_t isolated offline jet matched to the given trigger jet for a trigger jet requirement of 140 GeV.

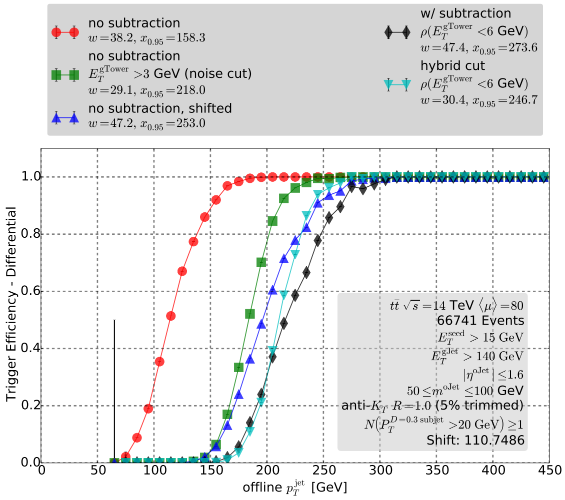

(a) at least 1 subjet

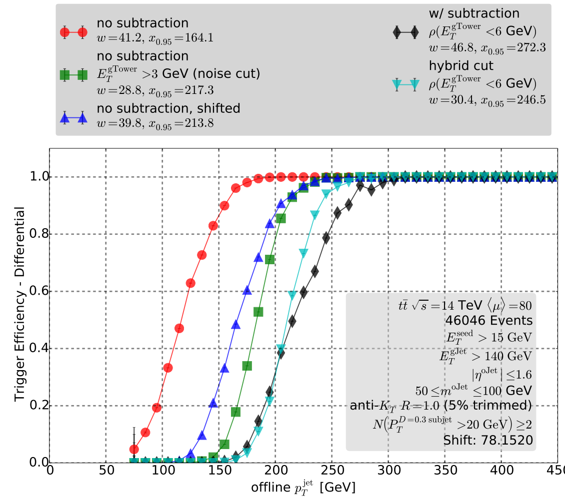

(b) at least 2 subjets

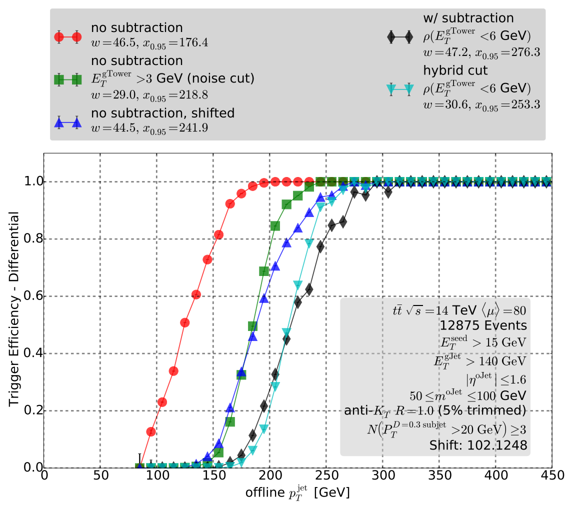

(c) at least 3 subjets

Figure 9.18: Trigger efficiency curves for the five different pile-up mitigation techniques. These are: no subtraction, no subtraction but a noise cut applied, no subtraction and simply shifted, with pile-up subtraction, and a hybrid cut. The legend reports the width of the turn-on w and the location of the plateau at 95% $x_{0.95}$. The efficiency is reported as a function of the large-R $R = 1.0$ anti-k_t isolated offline jet matched to the given trigger jet for a trigger jet requirement of 140 GeV. An additional selection on the mass of the offline jet is required to be within 50–100 GeV to enhance hadronic W-bosons.

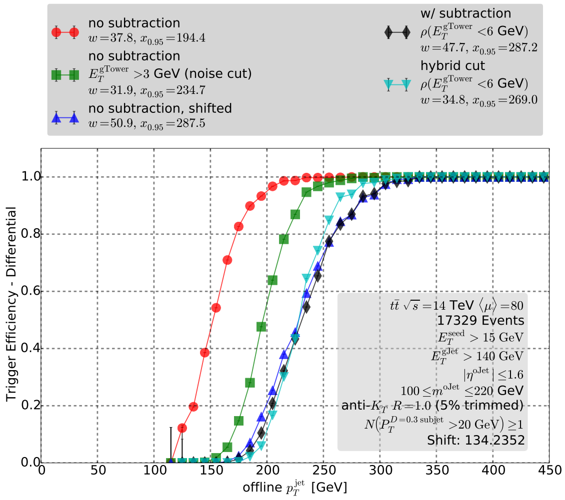

(a) at least 1 subjet

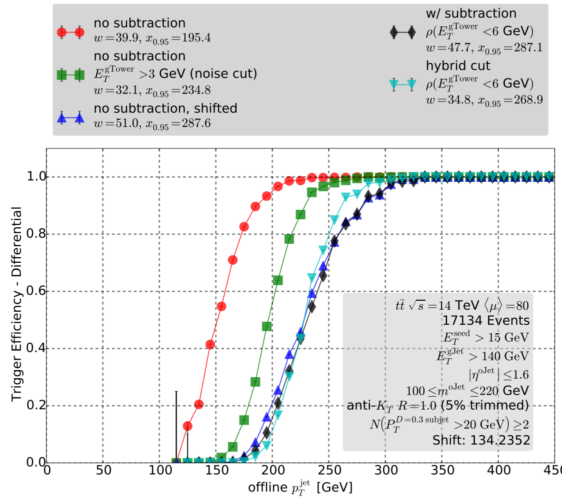

(b) at least 2 subjets

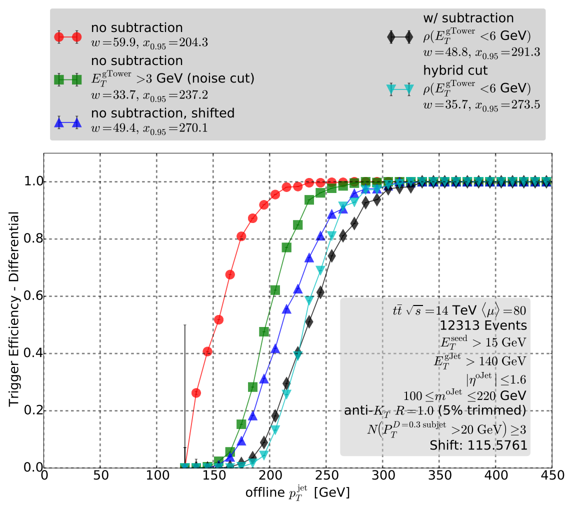

(c) at least 3 subjets

Figure 9.19: Trigger efficiency curves for the five different pile-up mitigation techniques. These are: no subtraction, no subtraction but a noise cut applied, no subtraction and simply shifted, with pile-up subtraction, and a hybrid cut. The legend reports the width of the turn-on w and the location of the plateau at 95% $x_{0.95}$. The efficiency is reported as a function of the large-R $R = 1.0$ anti-k_t isolated offline jet matched to the given trigger jet for a trigger jet requirement of 140 GeV. An additional selection on the mass of the offline jet is required to be within 100–200 GeV to enhance hadronic tops.

9.4.3 Substructure Studies

Now we are on the last series of upgrade studies that are presented in this thesis. All along, the jets that have been formed were often seeded by a single gTower above some particular E_{T} threshold, usually 15 GeV for the studies shown so far. However, if we think about the representation of a $t\bar{t}$ decay and its parton shower, it seems that the most energetic gTowers inside a reconstructed trigger jet should correspond with the subjets. Therefore, it's highly motivated to try and see if it is possible to identify trigger jets with significant substructure using the kinematics of the gTowers themselves. The first thing is to look at the correlation between leading gTower in each trigger jet that was reconstructed as shown in fig. 9.20 which shows a particularly strong correlation between the subjets of an offline jet and the leading gTowers in the associated trigger jet. This indicates that there is potentially some leverage to construct a discriminating variable for identifying subjets.

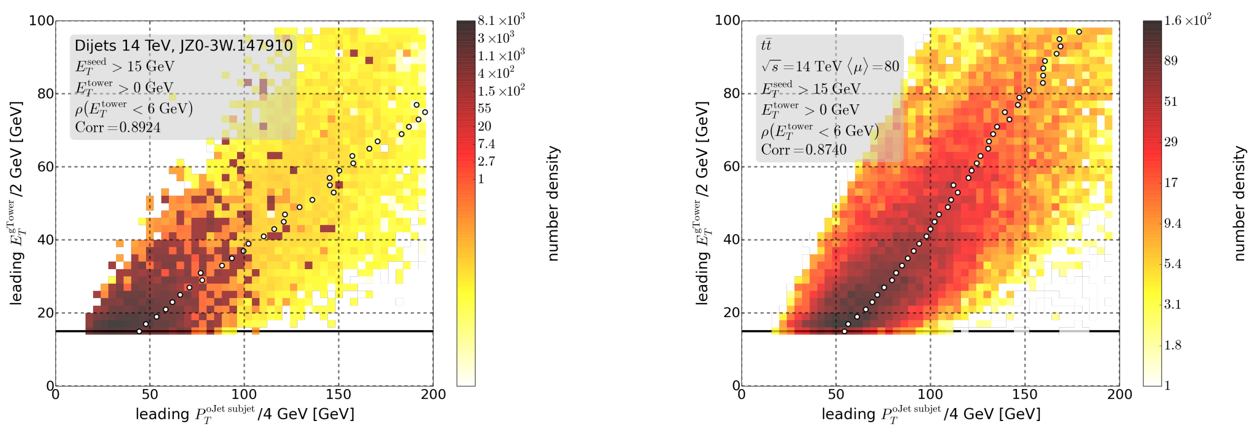

(a) dijets (b) $t\bar{t}$

Figure 9.20: Correlations of the energy between leading gTower and the matched offline jet's leading subjet for (a) QCD multijet and (b) $t\bar{t}$ monte-carlo simulated events with $\langle\mu\rangle = 80$ at a center-of-mass energy of $\sqrt{s} = 14\,\mathrm{TeV}$. The trigger jets are seeded with gTowers with $E_{\mathrm{T}} > 15\,\mathrm{GeV}$ and pile-up corrected using an upper threshold of 6 GeV. Notice that there is a nice average linearity and a relatively strong correlation (¿ 85%) for both monte-carlo samples. For multijet events, the leading gTower contains a majority of the energy of the offline jet, while for $t\bar{t}$ this is lower as expected for jets with significant substructure and energy spread out more.

So given all this information, the next straightforward study is to understand the gTower energy and the fraction of the total trigger jet energy as a function of exclusive binning in the number of subjets in the offline jet. This is a bit of a mouthful and this is shown in fig. 9.21. This is an enormously rich plot to breakdown. First, one can look at just the leading gTower in the event ("gTower 0") and can potentially apply a high, inverted selection on its energy to suppress dijet-like events where the offline jets only have one subjet. This is a preliminary study that needs to be explored further.

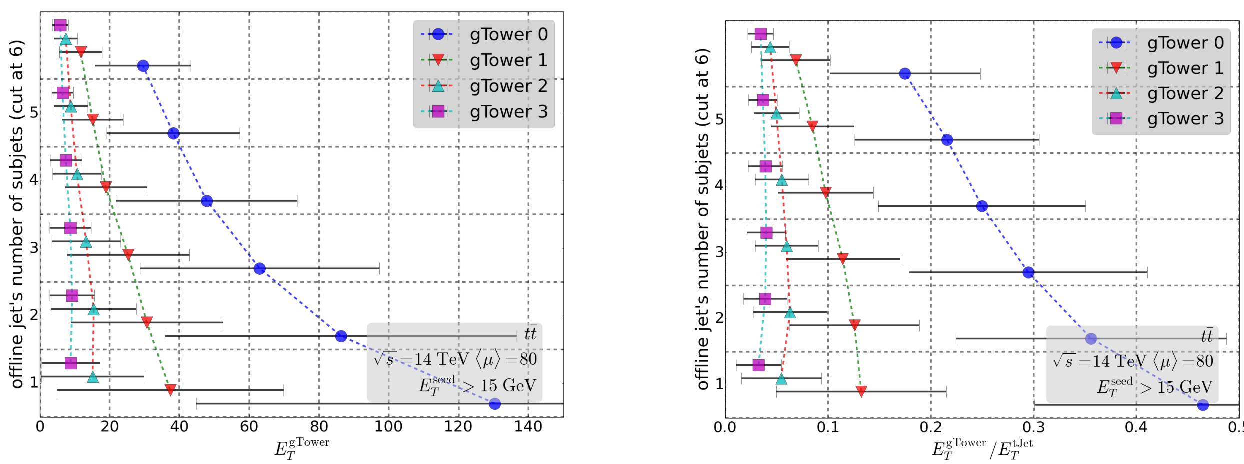

(a) tower energy

(b) fraction of trigger jet energy

Figure 9.21: Distributions of the (a) gTower energy and (b) fraction of gFEX trigger jet energy carried by each of the leading towers in the given jet. The y-axis is exclusive binning in the number of subjets of the matched, isolated, reconstructed offline jet. Dashed lines connect points which map the same type of gTower to understand the trends of the leading, subleading, etc. gTowers as you require more and more substructure in the offline jet. Each distribution of gTower energies for an offline subjet selection is fitted to a Gaussian and the mean is extracted and drawn as the marker, while the standard deviation is extracted and drawn as error bars.

So now that the leading four gTowers, sorted by $E_{\rm T}$, can be used as a proxy for subjets, can start to define a gFEX jet "subtower" multiplicity by $N(E_{\rm T}^{\rm tower} > X)$, the number of gTowers in a trigger jet greater than an $E_{\rm T}$ threshold. If we then consider $t\bar{t}$ a signal, and multijet as a background, we can start exploring trigger selections on "subtower multiplicity" in a way to maximize signal over background. This requires studying the trigger efficiency on signal and the fake rate on background, which is shown in fig. 9.22. In this study, isolated offline jets are matched to gFEX jets with $\Delta R < 1.0$, seeded with towers $E_{\mathrm{T}} > 15\,\mathrm{GeV}$ with no pile-up mitigation applied. The trigger selection applied is to require trigger jet $E_{\mathrm{T}} > 200\,\mathrm{GeV}$. In order to enhance the signal of $t\bar{t}$ to look purely at hadronic top decays that are fully captured, an offline jet mass cut is applied around the mass of the top quark $100\,\mathrm{GeV} < m^{\text{offline jet}} < 220\,\mathrm{GeV}$ and the p_{T} of the jet is required to be semi-boosted $250\,\mathrm{GeV} < p_{\mathrm{T}} < 500\,\mathrm{GeV}$.

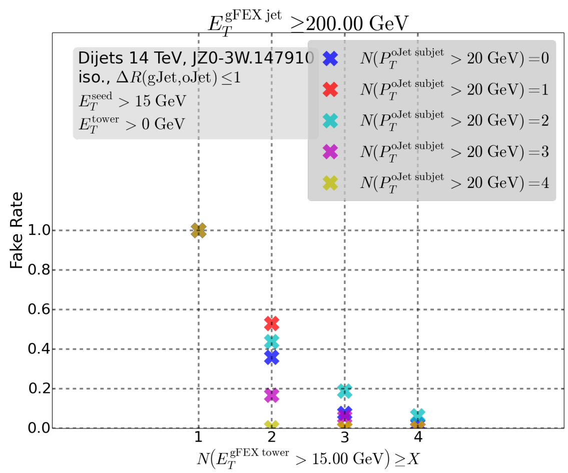

(a) dijets, fake rate

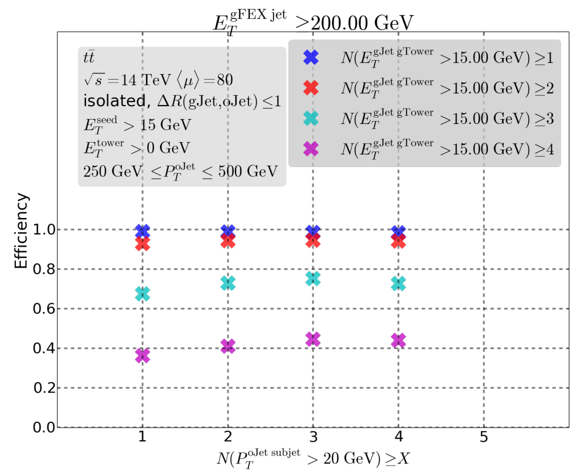

(b) $t\bar{t}$, efficiency

Figure 9.22: This is a plot of the (a) fake rate of dijet samples and (b) efficiency of the $t\bar{t}$ samples for monte-carlo simulated events with $\langle\mu\rangle = 80$ and a center-of-mass energy $\sqrt{s} = 14\,\mathrm{TeV}$. (a) is the background fake rate where a gFEX trigger jet E_{T} selection is applied to the denominator and numerator and a "subtower" multiplicity is applied to the numerator. (b) is the signal efficiency where the offline selection detailed in the plot is applied to the numerator and denominator and the trigger selection listed is applied to the numberator.

To test your understanding of fig. 9.22, let's walk through a single point in both background and signal. Take signal for a second and let's think about requiring that the offline jet has one subjet with $p_{\mathrm{T}} > 20\,\mathrm{GeV}$. The probability of finding more than one gTowers with $E_{\mathrm{T}} > 15\,\mathrm{GeV}$ goes down as we require more gTowers, and therefore the efficiency goes down as well in that particular column. Now take the background and again, think about requiring four subjets in the offline jet with $p_{\mathrm{T}} > 20\,\mathrm{GeV}$. As we increase the "subtower multiplicity" trigger selection in the numerator, the rate falls down, as it becomes less and less likely to find enough gTowers with sufficient energy. In particular, for dijet events where there is very little substructure to begin with, a dijet event that has many offline subjets will have many low energy subjets, compared to a dijet with less subjets each with higher energy. This is why the rate of dijet events with more offline jets falls off more sharply.

So now that we have a fake rate and a signal efficiency, we can combine the two into a single plot shown in fig. 9.23. This plot shows the signal efficiency as a function of the background "fake rate" (with no offline selection on the background). To test your understanding of this combination, a 6.3% background "fake rate" with 66% signal efficiency corresponds to $N(E_{\mathrm{T}}^{\mathrm{tower}} > 15\,\mathrm{GeV}) \geq 3$ which is a point that corresponds with boosted top quark decays! Precisely the kind of signal that my thesis analysis is sensitive to, but with a designed trigger that enables me to enhance the efficiency of selecting events while suppressing background, or uninteresting, events. Further study needs to be done to quantify the rate of the trigger given a trigger selection such as specified.

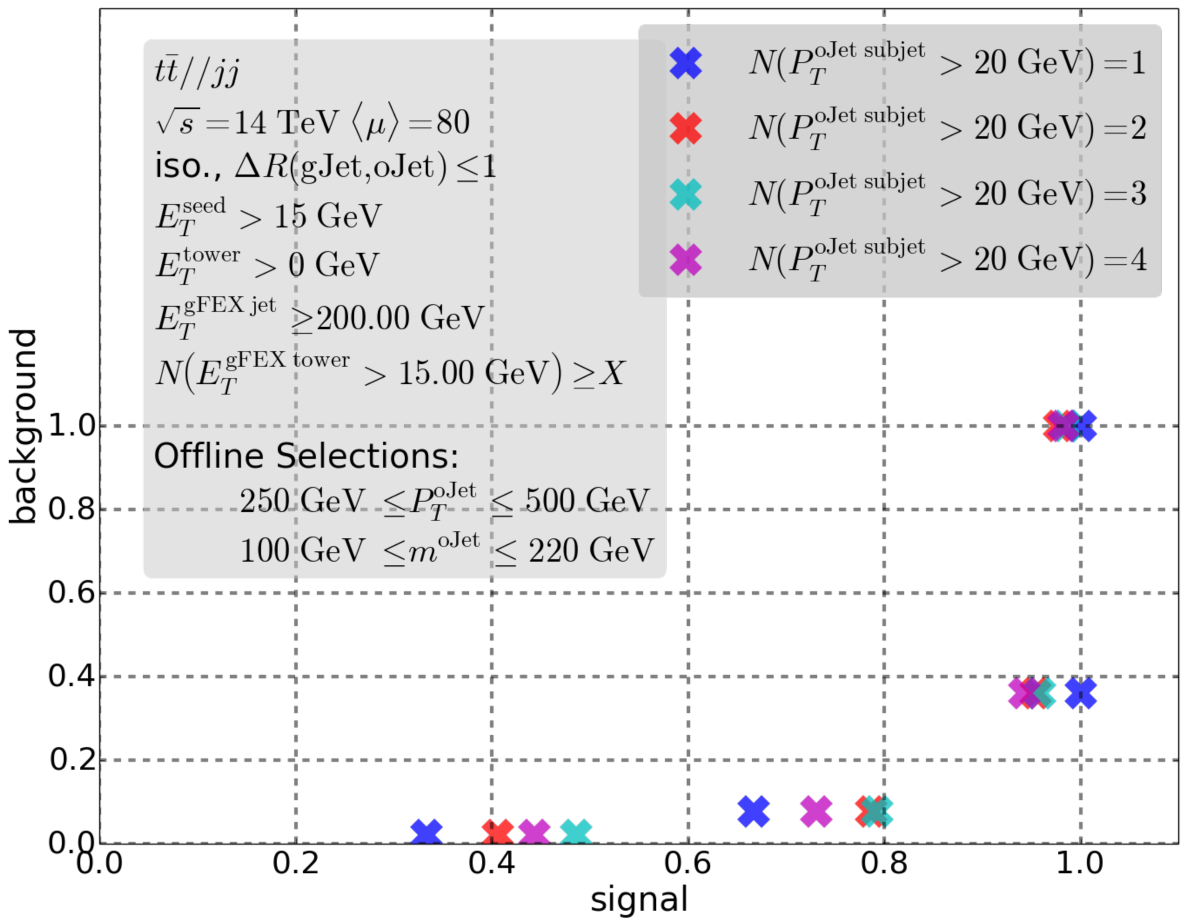

Figure 9.23: The signal efficiency is shown as a function of the background "fake rate" from fig. 9.22.

Glossary

ATLAS a general-purpose detector at the LHC. 2

gBlock Group of contiguous gTowers. Most have a size of 0.6×0.6 in $\Delta\phi \times \Delta\eta$.. 16

gFEX global Feature EXtractor.

gTower Tower, formed by summing electromagnetic & hadronic gCaloTowers, as used on the gFEX . Most have a size of 0.2×0.2 in $\Delta\phi \times \Delta\eta$.. 5–7, 11–18, 21–23, 27, 31–34

HLT High-Level Trigger. 21

L1 Level-1. 1, 3, 19

L1Calo L1 calorimeter trigger. 1, 23

large-R large-radius. 2

LHC Large Hadron Collider. 21

Bibliography

[1] Michael Begel et al. *Global Feature Extractor of the Level-1 Calorimeter Trigger: ATLAS TDAQ Phase-I Upgrade gFEX Final Design Report*. Tech. rep. ATL-COM-DAQ-2016-184. Geneva: CERN, Nov. 2016. URL: https://cds.cern.ch/record/2233958 (cit. on p. 1).

[2] *Letter of Intent for the Phase-I Upgrade of the ATLAS Experiment*. Tech. rep. CERN-LHCC-2011-012. LHCC-I-020. Geneva: CERN, Nov. 2011. URL: https://cds.cern.ch/record/1402470 (cit. on p. 1).

[3] ATLAS Collaboration. *Performance of shower deconstruction in ATLAS*. ATLAS-CONF-2014-003. 2014. URL: https://cds.cern.ch/record/1648661 (cit. on p. 3).

[4] ATLAS Collaboration. *Performance of boosted top quark identification in 2012 ATLAS data*. ATLAS-CONF-2013-084. 2013. URL: https://cds.cern.ch/record/1571040 (cit. on p. 4).

[5] ATLAS Collaboration. *Global Feature Extraction (gFEX) Performance Plots ATL-COM-DAQ-2014-087*. [Online; accessed 10-April-2018]. 2015. URL: https://twiki.cern.ch/twiki/bin/view/AtlasPublic/JetTriggerPublicResults (cit. on pp. 20, 23).

[6] M (CERN) Aleksa et al. *ATLAS Liquid Argon Calorimeter Phase-I Upgrade Technical Design Report*. Tech. rep. CERN-LHCC-2013-017. ATLAS-TDR-022. Final version presented to December 2013 LHCC. Sept. 2013. URL: https://cds.cern.ch/record/1602230 (cit. on p. 20).

[7] ATLAS Collaboration. *Pile-up subtraction and suppression for jets in ATLAS*. ATLAS-CONF-2013-083. 2013. URL: https://cds.cern.ch/record/1570994 (cit. on p. 23).